Editors' Suggestion

High-Efficiency Loading of 2400 Ytterbium Atoms in Optical Tweezer Arrays

Jiawen Zhu,[1,*] Changfeng Chen,[1,*] Li Zhou,[1] Xiangru Xie,[1] Chenyang Jiang,[1] Zhuoli Ding,[1] Fan Wu,[1] Fan Yang,[2] Guoqing Wang,[3] Qihuang Gong,[1,2,4,5] Peng Zhang,[6,7] Sheng Zhang,[1,†] and Pai Peng[1,4,‡]

[1]State Key Laboratory for Artificial Microstructure and Mesoscopic Physics and Frontiers Science Center for Nano-optoelectronics, School of Physics, Peking University, Beijing 100871, China
[2]Hefei National Laboratory, Hefei 230088, China
[3]International Center for Quantum Materials, School of Physics, Peking University, Beijing 100871, China
[4]Collaborative Innovation Center of Extreme Optics, Shanxi University, Taiyuan 030006, China
[5]Peking University Yangtze Delta Institute of Optoelectronics, Nantong, Jiangsu 226010, China
[6]School of Physics, Renmin University of China, Beijing 100872, China
[7]Key Laboratory of Quantum State Construction and Manipulation (Ministry of Education), Renmin University of China, Beijing 100872, China

(Received 24 March 2026; revised 12 June 2026; accepted 8 July 2026; published 4 August 2026)

Neutral atom arrays have emerged as a powerful platform for quantum computation, simulation, and metrology. Among them, alkaline-earth-like atoms exhibit distinct advantages, including long coherence time, high-fidelity Rydberg gates, and erasure correction for efficient quantum error correction. However, their scalability has lagged behind that of the alkali atoms. Here, we report 2400 ytterbium-174 atoms trapped in an optical tweezer array with enhanced loading efficiency of 83.5(1)% via blue-detuned light-assisted collisions. We develop a quantitative model of the collision dynamics and find good agreement between the calculated inelastic collision rates and the experimentally measured loading efficiencies. Notably, the loading efficiency is largely maintained for array sizes ranging from dozens to thousands, exhibiting excellent scalability. We further demonstrate that the enhancement exists robustly across a range of interatomic potentials, suggesting its utility for other atomic species. To establish the capability of the ^{174}Yb arrays toward universal quantum computation, we propose to encode the qubit in the ground-clock state manifold and estimate a 99.9% two-qubit gate fidelity with experimentally feasible parameters. Our work advances the prospects for realizing large-scale quantum computers using alkaline-earth-like atoms.

DOI: 10.1103/bp6k-8zmd

Introduction—Neutral atoms in optical tweezer arrays have developed rapidly over the past decade, emerging as one of the most promising platforms for quantum information science [1–3]. The rapid advancement is largely driven by their exceptional scalability, featuring thousands of atomic qubits with high-fidelity controls [4–11]. Recently, significant progress has been made toward various applications. For quantum computation, major milestones include the realization of high-fidelity Rydberg gates [12–17] and the demonstration of key fault-tolerant quantum computing elements [18–21]. As programmable quantum simulators, atom arrays offer unprecedented access to strongly correlated many-body phenomena, from quantum criticality to exotic states like quantum spin liquids [22–28]. For precision metrology, the platform opens new frontiers for optical atomic clocks via quantum enhancement [29,30]. Furthermore, continuous innovations in the system architectures are unlocking new capabilities, such as coherent atom transport for nonlocal gates [31], dual-species arrays for low-crosstalk control [32–34], local optical gates for faster control [35–40], efficient interface to photons [41–48], and continuous reloading for rapid atom replenishment [4–6,49,50]. These advances establish neutral atom arrays as a versatile and powerful platform for exploring the frontiers of quantum science and technology.

Among various atomic species, alkaline-earth-like atoms with two valence electrons, such as ytterbium and strontium, offer unique advantages for quantum control. Pure nuclear spins provide excellent coherence for quantum information storage due to their isolation from environmental noise [51,52]. The metastable states form the cornerstone of optical clocks, one of the most precise tools in quantum metrology [29,30,53]. Qubits encoded in the metastable state enable robust single-photon Rydberg excitation [54–56], optical clock-state control [57–59], and midcircuit erasure conversion, which significantly reduces the resource overhead for quantum error correction [20,56,60–62]. However, an important challenge for alkaline-earth-like atom arrays is their limited size, as compared

[*]These authors contributed equally to this work.
[†]Contact author: sheng.physik@pku.edu.cn
[‡]Contact author: pengpai@pku.edu.cn

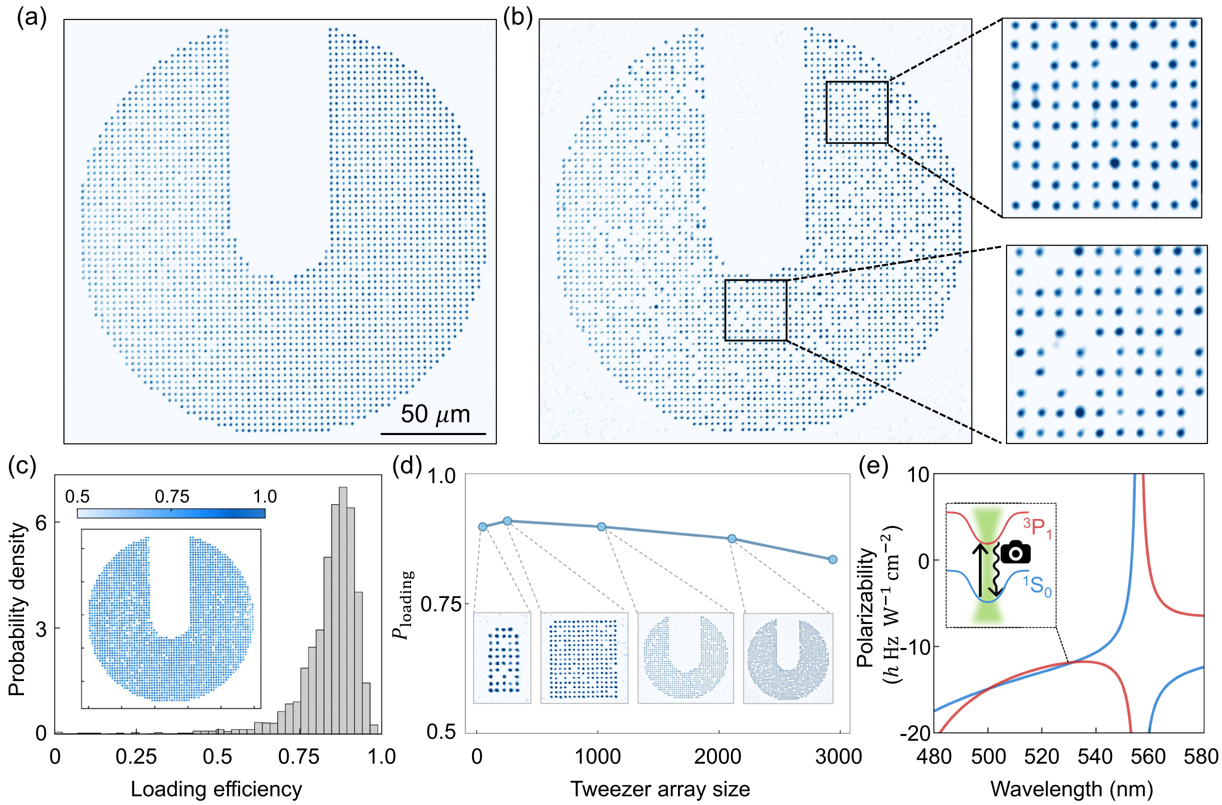

FIG. 1. (a) Averaged fluorescence image of a 2939-site array over 85 experimental trials. (b) Single-shot image of 2437 single atoms. Spatial high-pass filter is applied in (a) and (b). (c) A histogram presenting the site-resolved loading efficiency, with the inset illustrating the efficiency across the array. The average loading efficiency is 83.5(1)% with standard deviation of 10.3% across all sites. Data are collected from 85 images. (d) The loading efficiency for different array sizes with the same trap depth and tweezer spacing. The enhanced loading parameters are optimized for each array size. The highest and lowest loading efficiencies are 91.1(4)% and 83.5(7)%, respectively. Error bars are smaller than the marker. Insets show single-shot images of the corresponding array [image of the largest array is in (b)]. (e) Polarizabilities for the ground state $^1S_0$ (blue curve) and the excited state $^3P_1$ (red curve) of ^{174}Yb from numerical calculation (data of atomic levels from Ref. [68]), which are used for fluorescence imaging (inset). The optical tweezer operates at the magic wavelength of 532 nm. The enhanced loading in all plots is performed with π-polarized light, $I/I_{\rm sat} = 53$, a detuning of $\Delta = 2\pi \times 4$ MHz relative to the $m_J = 0$ state, and a 2.3 G magnetic field.

to alkali species with a record of 6100 atoms [7]. This is due to the low polarizability of alkaline-earth-like atoms at near-infrared wavelengths where high-power lasers are commercially available, therefore limiting the maximum number of optical tweezers with sufficient depth. Moreover, for an optical tweezer array of fixed size, the ~50% statistical single-atom loading efficiency imposes a stringent constraint on the number of trapped atoms. Blue-detuned light-assisted collision has been employed to enhance the loading efficiency for certain atomic species and array sizes up to 100 [51,63–67]. Up to now, it has been an open question whether the method can be broadly applied to different species or much larger arrays.

In this Letter, we demonstrate a high-efficiency preparation of the largest alkaline-earth-like atom array in optical tweezers, comprising over 2400 ytterbium-174 atoms [Figs. 1(a) and 1(b)]. This is enabled by the efficient trapping and high-fidelity imaging of ytterbium-174 atoms in 532 nm optical tweezers. We achieve an enhanced loading efficiency of 83.5(1)% in ~3000 optical tweezers [Fig. 1(c)]. The high loading efficiency is maintained from a few tens to thousands of tweezers [Fig. 1(d)], highlighting the scalability of the enhanced loading method to large arrays. To understand the light-assisted collision dynamics, we develop a quantitative model that directly links the inelastic collision rate to the observed loading efficiency, yielding good agreement with experiment. By engineering different interatomic potentials, we demonstrate that enhanced loading does not necessarily require the globally repulsive potentials in earlier experiments [51,63–67] but can also be achieved with partially repulsive potentials accessible in generic two-level systems, thereby broadening its applicability across atomic species. For quantum controls of ytterbium-174 atoms, we propose to encode the qubit in the ground-clock state manifold. From numerical simulation and comparison to the ^{171}Yb isotope, we estimate that single-qubit gate fidelity of 99.8% and two-qubit gate fidelity of 99.9% can be achieved with experimentally realistic parameters. Our work realizes large-scale alkaline-earth-like atom arrays with high loading efficiency. In combination with their estimated long coherence time and high-fidelity controls, alkaline-earth-like atom arrays hold great potential to unlock tremendous capabilities toward universal quantum computation.

Large-scale ^{174}Yb atom arrays—Here, we introduce the main results and methods regarding the large-scale atom arrays. We first cool ^{174}Yb atoms using a two-stage laser cooling setup, resulting in an ensemble of atoms at the Doppler temperature of 5 μK in the magneto-optical trap (MOT). The detailed implementation is described in Supplemental Material Sec. I [69]. Static tweezer arrays are generated via a programmable spatial light modulator (SLM) using a weighted Gerchberg-Saxton algorithm [74–76]. A 532 nm laser is phase modulated by the SLM and then focused by a microscope objective (numerical aperture = 0.6, field of view = 500 μm), creating arrays of up to 2939 sites. The averaged image is shown in Fig. 1(a), and a single-shot image is shown in Fig. 1(b). The tweezer spacing is set to 2.8 μm, and the trap depth is $U_0/\hbar \approx 2\pi \times 4$ MHz (3 mW per tweezer, estimated from $^3P_1$ tensor light shift).

Cooling and fluorescence imaging of atoms are performed on the $|^1S_0\rangle \rightarrow |^3P_1, m_J = 0\rangle$ intercombination line. This transition is magic at the 532 nm tweezer wavelength [77]; i.e., ac Stark shifts of the ground and excited states are identical [Fig. 1(e)]. The magic trap enables an imaging survival probability of 99.1(3)% and an imaging fidelity of 99.3(1)%.

Leveraging blue-detuned light-assisted collisions, we achieve a high loading efficiency, enabling the capture of more than 2400 atoms in a single experimental trial. The statistics and spatial distribution of site-resolved loading efficiency are presented in Fig. 1(c), showing an average loading efficiency of 83.5(1)%, where the lower-efficiency sites are mainly attributed to local trap quality that could be mitigated using the method described in Ref. [7]. We measure loading efficiency for different array sizes and observe over 80% loading efficiency from tens to thousands of optical tweezers [Fig. 1(d)]. The moderate decrease for larger arrays is likely due to reduced effective atom density in the target plane [51], arising from atom capture by residual out-of-plane traps during loading.

High-efficiency loading—Let us first discuss conventional single-atom preparation methods. A red-detuned laser induces light-assisted collisions that expel two atoms out of the tweezer. The combination of the random initial loading number and the two-to-zero collisional loss imposes a ≈50% upper bound on the single-atom loading efficiency. For atoms with a repulsive interatomic potential, a blue-detuned collision laser has been used to improve the loading efficiency in certain cases [51,63–67]. However, it remains elusive whether this method can be applied to other atomic species and what the optimal parameters for loading enhancement are.

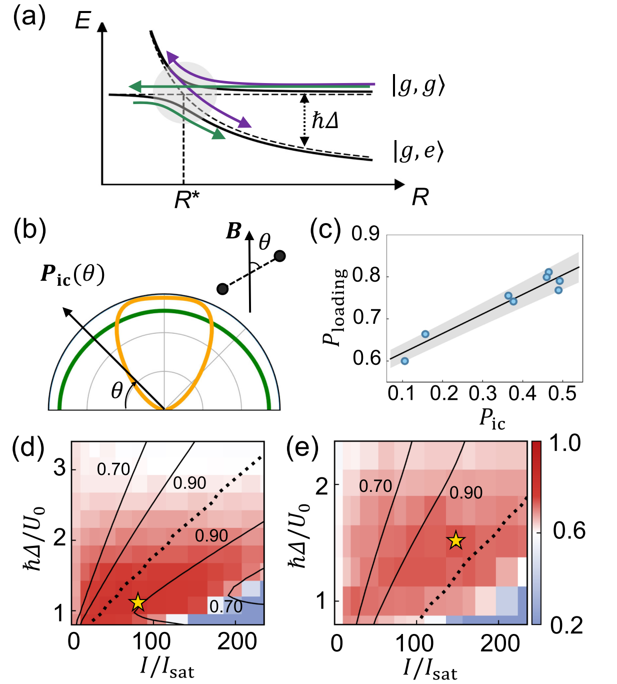

FIG. 2. (a) The enhanced loading mechanism. The solid black curves represent the molecular eigenstates in the rotating frame of the blue-detuned laser, with the gray region highlighting the crossing point. Green and purple arrows mark two pathways for inelastic collision. (b) The angular distribution of the simulated inelastic collision probability P_{ic} as a function of θ, with θ being the angle between the interatomic displacement and the quantization axis [$I/I_{sat} = 100$, $\hbar\Delta/U_0 = 1.35$, close to the optimal point in (d) and (e)]. The green curve corresponds to a globally repulsive potential, while the orange curve corresponds to a potential that is repulsive only around $\theta = 90°$. (c) Linear relationship between the optimal $P_{loading}$ and P_{ic} for different light polarizations and magnetic fields [data from (d),(e), and Supplemental Material Figs. S3(a) and S3(b) [69]]. Both $P_{loading}$ and P_{ic} are maximized over $\hbar\Delta/U_0 \in [1, 2]$ and $I/I_{sat} \leq 150$. The black line shows a linear fit, with $\pm 1\sigma$ uncertainty marked by the gray shade. The error bars are smaller than the markers. (d), (e) The loading efficiency of the globally and partially repulsive potential, respectively. The loading enhancement time is 500 ms. The stars label the maximum $P_{loading}$ [81.1(4)% in (d) and 74.1 (7)% in (e)]. The black dots (contours) mark the highest P_{ic} (90% and 70% of the highest P_{ic}) for each detuning. The detuning is relative to the single-atom energy level coupled by the collision light, i.e., $m_J = \pm 1$ in (d) and $m_J = 0$ in (e). All data presented in this figure are collected with an array size of 2107.

Here, we present a quantitative model of the blue-detuned light-assisted collision process that answers the above questions. Figure 2(a) shows the interatomic potential in the rotating frame of the collision laser frequency, considering one ground state $|g\rangle$ and one excited state $|e\rangle$ for simplicity. During the collision process, an atom pair starting from the $|g, g\rangle$ state passes through the $|g, g\rangle$-$|g, e\rangle$ crossing twice. If *one of the two passages is adiabatic and the other is nonadiabatic* [green and purple arrows in

Fig. 2(a)], an inelastic collision happens and the atom pair gains kinetic energy $\hbar\Delta$, with Δ being the laser detuning. When $\hbar\Delta \gtrsim U_{\mathrm{trap}}$, only one atom can escape from the trap, leading to a one-by-one atom loss until only a single atom remains [78]. We calculate the interatomic potential using the dipole-dipole interaction model and the inelastic collision probability P_{ic} by solving the Lindblad equation (Supplemental Material Sec. III [69]).

Next, we experimentally study the enhanced loading performance by engineering interatomic potentials. We realize two representative potentials—(i) a globally repulsive potential using mixed light polarizations under zero magnetic field [the green curve in Fig. 2(b)] and (ii) a partially repulsive potential using pure π polarization under 8.6 G field along the tweezer polarization direction [the orange curve in Fig. 2(b)]. We observe significant loading enhancement under both the globally and partially repulsive potentials [Figs. 2(d) and 2(e)]. We also find good agreement between the calculated P_{ic} and the measured loading efficiency, validating the theoretical model [Figs. 2(c)–2(e)]. The maximum loading efficiency achieved here is ~80%. The imperfection is because we apply a cooling light during collision (red detuned from the $|^1S_0\rangle \rightarrow |^3P_1, m_J = 0\rangle$ magic transition) to cool the remaining atom, which induces a finite two-to-zero loss probability as in the conventional red-detuned light-assisted collision process. Enhanced loading performance under other potentials can be found in Supplemental Material Fig. S3 [69].

Note that previous enhanced loading studies [51,63–67] utilize either Λ systems or multiple degenerate states where the interatomic potentials are globally repulsive, similar to the case in Fig. 2(d). Here, we find loading enhancement under partially repulsive potentials, which are attainable in generic two-level systems (Supplemental Material Sec. III [69]).

Characterization of atom loading and imaging—As the tweezer array size (82 μm radius) is larger than the MOT ($1/e^2$ radius of 48 μm), we rotate the position of the MOT to achieve a uniform loading by modulating the bias magnetic field. Figure 3(a) shows a significant improvement of initial loading efficiency with MOT rotation. More details about the rotating MOT method can be found in Supplemental Material Sec. I [69].

Next, we characterize the imaging fidelity. As the large optical tweezer array is inevitably associated with out-of-plane traps [7], fluorescence from atoms in those traps creates a strong background in the image. We apply spatial high-pass filters to eliminate this background following Ref. [8] (Supplemental Material Sec. II [69]). Figure 3(b) displays the statistics of fluorescence brightness for all sites in 1000 images. We use the same brightness threshold to determine the occupancy for all sites. Using the analysis method from Ref. [7], we estimate the average imaging fidelity of 99.3(1)% and the atom loss rate of 0.9(3)% per image. The spatial distribution of imaging fidelities across

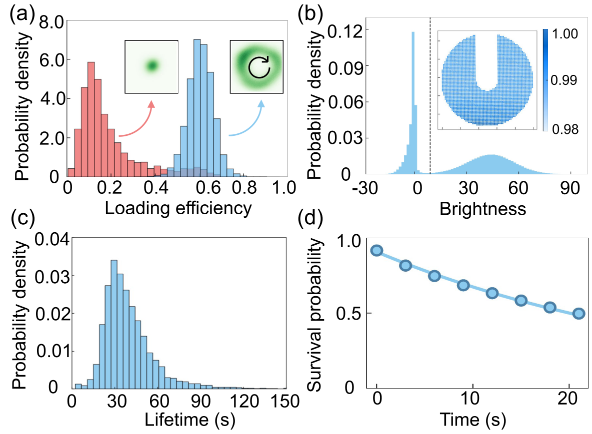

FIG. 3. (a) Initial loading efficiency distribution with (blue) and without (red) implementing the rotating MOT technique, prior to the enhanced loading step. The insets illustrate the fixed MOT and the rotating MOT. (b) Histogram of fluorescence brightness across all array sites. The two peaks of the bimodal distribution correspond to zero and one atom occupancy. The inset depicts the site-resolved imaging fidelity. The exposure time is 200 ms, limited by the background of out-of-plane atoms (Supplemental Material Sec. II [69]). Data are collected from 1000 images. (c) Probability density distribution of imaging lifetime across the array sites. (d) The average atom survival over all sites with respect to the imaging time, showing a lifetime of 35.1(5) s. All data presented in this figure are collected under the maximum array size of 2939.

the entire array is presented in the inset in Fig. 3(b). Imaging lifetime is determined by continuously shining the imaging light and measuring atom survival probabilities. The result is presented in Figs. 3(c) and 3(d) with an average imaging lifetime of 35.1(5) s, consistent with the atom loss rate measured above.

^{174}Yb gate scheme—To establish the large-scale ^{174}Yb atom arrays as quantum processors, we next present qubit encoding and quantum gate schemes. Compared to the commonly used ^{171}Yb isotope with well-studied nuclear spin qubits [56,59], ^{174}Yb has zero nuclear spin and, thus, lacks the nuclear spin qubits. Inspired by the *omg* encoding demonstrated in ^{171}Yb [59], we propose to encode qubits in the ground $^1S_0$ and clock $^3P_0$ states of ^{174}Yb atoms, as shown in Fig. 4(a). One advantage of this optical qubit is that $J = 0$ for both states, and, therefore, it is insensitive to magnetic field noise and tweezer polarization imperfections [20]. The 578 nm clock transition between qubit states can be excited with a magnetic field that mixes $^3P_0$ and $^3P_1$ [79]. For a 200 G magnetic field, 1 W laser power (2 W 578 nm laser is commercially available) with a beam waist of 9 μm can induce a Rabi frequency of $2\pi \times 110$ kHz. This is comparable to the 99.8% single-qubit gate in the ^{171}Yb case [59]. For the clock-state encoding, the corresponding magic trapping wavelength is 759 nm, where the polarizability and available laser power are smaller than those at 532 nm. Nevertheless, the available 759 nm optical power is not expected to be the limitation at the

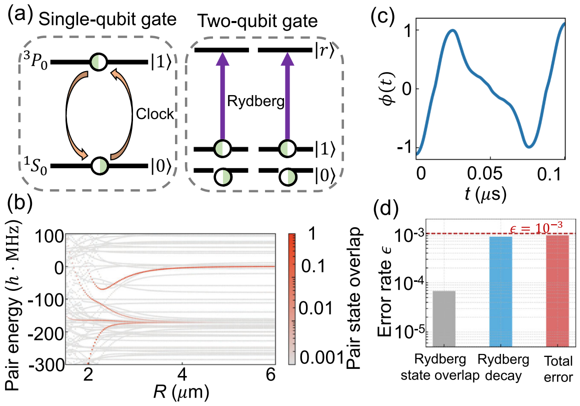

FIG. 4. (a) Level diagram of single- and two-qubit gates. (b) Calculated Rydberg-pair interaction potential for the state $|r\rangle = |\nu = 49.56, L = 0, J = 1, m_J = 1\rangle$ at a magnetic field of 200 G with atoms aligned perpendicular to the magnetic field. The color of each curve represents its overlap with the target pair state $|r, r\rangle$. (c) Laser phase of the time-optimal CZ gate, assuming an interatomic distance of 1.9 μm. (d) Numerical simulation of the two-qubit gate error rates.

demonstrated array scale, because clock-state storage can be achieved with much shallower traps (Supplemental Material Sec. V [69]).

For two-qubit gates, we propose to couple $^3P_0$ to $|r\rangle = |\nu = 49.56, L = 0, J = 1, m_J = 1\rangle$ Rydberg state, where ν, L, J, and m_J are the effective principal quantum number, orbital angular momentum, total angular momentum, and total angular momentum z component, respectively. This Rydberg excitation requires a 302 nm UV laser, where ~1 W power is commercially available. Assuming a 75 mW Rydberg laser inside the vacuum chamber and a beam waist of 12 μm, we estimate the Rabi frequency to be $2\pi \times 15$ MHz. We consider the fundamental errors of two-qubit Rydberg gates—Rydberg decay and excitation to nearby overlapping Rydberg pair states (Supplemental Material Sec. V [69]). We calculate the Rydberg pair state overlaps following the multichannel quantum defect model from Ref. [12] [Fig. 4(b)]. With the Rydberg state information, we then optimize a pulse for the controlled-Z (CZ) gate using the gradient ascent pulse engineering algorithm [80]. The resulting pulse is shown in Fig. 4(c). The simulated CZ gate fidelity is 99.91% (quantified using the Bell state fidelity), dominated by Rydberg decay. The results demonstrate that the gate fidelities of ^{174}Yb are well above the surface-code error-correction thresholds and are comparable to those of the commonly used ^{171}Yb isotope.

We note that the ^{174}Yb atom array is also promising for quantum simulations with the qubits encoded in the clock-Rydberg manifold [62]. Featuring large system sizes and high-fidelity Rydberg excitations, the ^{174}Yb atom array can simulate quantum many-body systems approaching the thermodynamic limit with high precision.

Conclusion and outlook—In summary, we realize alkaline-earth-like atom arrays comprising over 2400 ytterbium-174 atoms in optical tweezer arrays. We systematically investigate the enhanced loading mechanism for a range of array sizes and interatomic potentials, demonstrating its scalability to larger arrays and applicability to most atoms or molecules with dipole-dipole interactions [81,82]. We also propose a qubit encoding scheme using the ground and clock states of ^{174}Yb and estimate gate fidelities approaching 99.9%.

Further improvements of the array size can be achieved by reusing laser power via optical lattices or optical cavity arrays [46,50]. We also note that the light-assisted collisions between $J = 0$ and $J = 1$ states in this Letter are reminiscent of the microwave shielding of ultracold polar molecules in the lowest rotational states with angular momenta 0 and 1 [83–89]. Therefore, our work might provide mutual reference and promotion between the single-atom preparation in atom arrays and microwave shielding of ultracold molecules. Finally, the integration of loading enhancement, rapid SLM rearrangement [8], and continuous reloading techniques [4–6,49] would enable large-scale, defect-free, and sustainable ^{174}Yb atom arrays. The combination of the large qubit number and estimated high gate fidelities makes the ^{174}Yb arrays a promising platform for quantum error correction and logical operations at large scale [19].

Acknowledgments—We thank Wenjun Zhang for fruitful discussions, Rongpei Zhu for the help with the laser setups, and Hao Zhang and Yue Jiang for the help with objective tests. This work was supported by the Quantum Science and Technology-National Science and Technology Major Project under Grants No. 2024ZD0301600 and No. 2025ZD0300400, the National Natural Science Foundation of China under Grants No. 12474479 and No. 12504573, the Beijing Natural Science Foundation under Grant No. F251004, the Innovation Program for Quantum Science and Technology under Grant No. 2023ZD0300700, the National Key Research and Development Program of China under Grant No. 2022YFA1405300, the China Postdoctoral Science Foundation under Grants No. 2024M760064 and No. 2025T180934, and the Postdoctoral Fellowship Program of CPSF under Grant No. GZB20250790.

Data availability—The data that support the findings of this study are available [90].

[1] M. Endres, H. Bernien, A. Keesling, H. Levine, E. R. Anschuetz, A. Krajenbrink, C. Senko, V. Vuletic, M. Greiner, and M. D. Lukin, Atom-by-atom assembly of defect-free one-dimensional cold atom arrays, Science **354**, 1024 (2016).

[2] D. Barredo, S. de Léséleuc, V. Lienhard, T. Lahaye, and A. Browaeys, An atom-by-atom assembler of defect-free arbitrary two-dimensional atomic arrays, Science **354**, 1021 (2016).

[3] H. Kim, W. Lee, H.-g. Lee, H. Jo, Y. Song, and J. Ahn, In situ single-atom array synthesis using dynamic holographic optical tweezers, Nat. Commun. **7**, 13317 (2016).

[4] M. A. Norcia, H. Kim, W. B. Cairncross, M. Stone, A. Ryou, M. O. Jaffe, M. Brown, K. Barnes, P. Battaglino, T. Bohdanowicz *et al.*, Iterative assembly of ^{171}Yb atom arrays with cavity-enhanced optical lattices, PRX Quantum **5**, 030316 (2024).

[5] F. Gyger, M. Ammenwerth, R. Tao, H. Timme, S. Snigirev, I. Bloch, and J. Zeiher, Continuous operation of large-scale atom arrays in optical lattices, Phys. Rev. Res. **6**, 033104 (2024).

[6] N.-C. Chiu, E. C. Trapp, J. Guo, M. H. Abobeih, L. M. Stewart, S. Hollerith, P. L. Stroganov, M. Kalinowski, A. A. Geim, S. J. Evered *et al.*, Continuous operation of a coherent 3,000-qubit system, Nature (London) **646**, 1075 (2025).

[7] H. J. Manetsch, G. Nomura, E. Bataille, X. Lv, K. H. Leung, and M. Endres, A tweezer array with 6,100 highly coherent atomic qubits, Nature (London) **647**, 60 (2025).

[8] R. Lin, H.-S. Zhong, Y. Li, Z.-R. Zhao, L.-T. Zheng, T.-R. Hu, H.-M. Wu, Z. Wu, W.-J. Ma, Y. Gao *et al.*, AI-enabled parallel assembly of thousands of defect-free neutral atom arrays, Phys. Rev. Lett. **135**, 060602 (2025).

[9] G. Pichard, D. Lim, E. Bloch, J. Vaneecloo, L. Bourachot, G.-J. Both, G. Mériaux, S. Dutartre, R. Hostein, J. Paris *et al.*, Rearrangement of individual atoms in a 2000-site optical-tweezer array at cryogenic temperatures, Phys. Rev. Appl. **22**, 024073 (2024).

[10] A. Holman, Y. Xu, X. Sun, J. Wu, M. Wang, Z. Zhu, B. Seo, N. Yu, and S. Will, Trapping of single atoms in metasurface optical tweezer arrays, Nature (London) **649**, 859 (2026).

[11] L. Pause, L. Sturm, M. Mittenbühler, S. Amann, T. Preuschoff, D. Schäffner, M. Schlosser, and G. Birkl, Supercharged two-dimensional tweezer array with more than 1000 atomic qubits, Optica **11**, 222 (2024).

[12] M. Peper, Y. Li, D. Y. Knapp, M. Bileska, S. Ma, G. Liu, P. Peng, B. Zhang, S. P. Horvath, A. P. Burgers *et al.*, Spectroscopy and modeling of ^{171}Yb Rydberg states for high-fidelity two-qubit gates, Phys. Rev. X **15**, 011009 (2025).

[13] S. J. Evered, D. Bluvstein, M. Kalinowski, S. Ebadi, T. Manovitz, H. Zhou, S. H. Li, A. A. Geim, T. T. Wang, N. Maskara *et al.*, High-fidelity parallel entangling gates on a neutral-atom quantum computer, Nature (London) **622**, 268 (2023).

[14] R. B.-S. Tsai, X. Sun, A. L. Shaw, R. Finkelstein, and M. Endres, Benchmarking and fidelity response theory of high-fidelity Rydberg entangling gates, PRX Quantum **6**, 010331 (2025).

[15] A. Senoo, A. Baumgärtner, J. W. Lis, G. M. Vaidya, Z. Zeng, G. Giudici, H. Pichler, and A. M. Kaufman, High-fidelity entanglement and coherent multi-qubit mapping in an atom array, Nat. Phys. **22**, 903 (2026).

[16] J. A. Muniz, M. Stone, D. T. Stack, M. Jaffe, J. M. Kindem, L. Wadleigh, E. Zalys-Geller, X. Zhang, C.-A. Chen, M. A. Norcia *et al.*, High-fidelity universal gates in the ^{171}Yb ground-state nuclear-spin qubit, PRX Quantum **6**, 020334 (2025).

[17] A. Radnaev, W. Chung, D. Cole, D. Mason, T. Ballance, M. Bedalov, D. Belknap, M. Berman, M. Blakely, I. Bloomfield *et al.*, Universal neutral-atom quantum computer with individual optical addressing and nondestructive readout, PRX Quantum **6**, 030334 (2025).

[18] D. Bluvstein, S. J. Evered, A. A. Geim, S. H. Li, H. Zhou, T. Manovitz, S. Ebadi, M. Cain, M. Kalinowski, D. Hangleiter *et al.*, Logical quantum processor based on reconfigurable atom arrays, Nature (London) **626**, 58 (2024).

[19] H. Zhou, C. Zhao, M. Cain, D. Bluvstein, N. Maskara, C. Duckering, H.-Y. Hu, S.-T. Wang, A. Kubica, and M. D. Lukin, Low-overhead transversal fault tolerance for universal quantum computation, Nature (London) **646**, 303 (2025).

[20] B. Zhang, G. Liu, G. Bornet, S. P. Horvath, P. Peng, S. Ma, S. Huang, S. Puri, and J. D. Thompson, Logical qubits with erasure conversion using metastable neutral atoms, Nat. Phys. **22**, 910 (2026).

[21] B. W. Reichardt, A. Paetznick, D. Aasen, I. Basov, J. M. Bello-Rivas, P. Bonderson, R. Chao, W. van Dam, M. B. Hastings, R. V. Mishmash *et al.*, Fault-tolerant quantum computation with a neutral atom processor, arXiv: 2411.11822.

[22] F. Fang, K. Wang, V. S. Liu, Y. Wang, R. Cimmino, J. Wei, M. Bintz, A. Parr, J. Kemp, K.-K. Ni *et al.*, Probing critical phenomena in open quantum systems using atom arrays, Science **390**, 601 (2025).

[23] C. Chen, G. Emperauger, G. Bornet, F. Caleca, B. Gély, M. Bintz, S. Chatterjee, V. Liu, D. Barredo, N. Y. Yao *et al.*, Spectroscopy of elementary excitations from quench dynamics in a dipolar XY Rydberg simulator, Science **389**, 483 (2025).

[24] T. Zhang, H. Wang, W. Zhang, Y. Wang, A. Du, Z. Li, Y. Wu, C. Li, J. Hu, H. Zhai *et al.*, Observation of near-critical Kibble-Zurek scaling in Rydberg atom arrays, Phys. Rev. Lett. **135**, 093403 (2025).

[25] D.-S. Xiang, Y.-W. Zhang, H.-X. Liu, P. Zhou, D. Yuan, K. Zhang, S.-Y. Zhang, B. Xu, L. Liu, Y. Li *et al.*, Observation of quantum information collapse-and-revival in a strongly-interacting Rydberg atom array, Nat. Commun. (2026).

[26] G. Semeghini, H. Levine, A. Keesling, S. Ebadi, T. T. Wang, D. Bluvstein, R. Verresen, H. Pichler, M. Kalinowski, R. Samajdar *et al.*, Probing topological spin liquids on a programmable quantum simulator, Science **374**, 1242 (2021).

[27] X. Liang, Z. Yue, Y.-X. Chao, Z.-X. Hua, Y. Lin, M. K. Tey, and L. You, Observation of anomalous information scrambling in a Rydberg atom array, Phys. Rev. Lett. **135**, 050201 (2025).

[28] M. Qiao, G. Emperauger, C. Chen, L. Homeier, S. Hollerith, G. Bornet, R. Martin, B. Gély, L. Klein, D. Barredo *et al.*, Realization of a doped quantum antiferromagnet in a Rydberg tweezer array, Nature (London) **644**, 889 (2025).

[29] A. Cao, W. J. Eckner, T. Lukin Yelin, A. W. Young, S. Jandura, L. Yan, K. Kim, G. Pupillo, J. Ye, N. Darkwah Oppong *et al.*, Multi-qubit gates and Schrödinger cat states in an optical clock, Nature (London) **634**, 315 (2024).

[30] R. Finkelstein, R. B.-S. Tsai, X. Sun, P. Scholl, S. Direkci, T. Gefen, J. Choi, A. L. Shaw, and M. Endres, Universal quantum operations and ancilla-based read-out for tweezer clocks, Nature (London) **634**, 321 (2024).

[31] D. Bluvstein, H. Levine, G. Semeghini, T. T. Wang, S. Ebadi, M. Kalinowski, A. Keesling, N. Maskara, H. Pichler, M. Greiner *et al.*, A quantum processor based on coherent transport of entangled atom arrays, Nature (London) **604**, 451 (2022).

[32] C. Sheng, J. Hou, X. He, K. Wang, R. Guo, J. Zhuang, B. Mamat, P. Xu, M. Liu, J. Wang *et al.*, Defect-free arbitrary-geometry assembly of mixed-species atom arrays, Phys. Rev. Lett. **128**, 083202 (2022).

[33] K. Singh, S. Anand, A. Pocklington, J. T. Kemp, and H. Bernien, Dual-element, two-dimensional atom array with continuous-mode operation, Phys. Rev. X **12**, 011040 (2022).

[34] S. Anand, C. E. Bradley, R. White, V. Ramesh, K. Singh, and H. Bernien, A dual-species Rydberg array, Nat. Phys. **20**, 1744 (2024).

[35] T. Graham, Y. Song, J. Scott, C. Poole, L. Phuttitarn, K. Jooya, P. Eichler, X. Jiang, A. Marra, B. Grinkemeyer *et al.*, Multi-qubit entanglement and algorithms on a neutral-atom quantum computer, Nature (London) **604**, 457 (2022).

[36] B. Zhang, P. Peng, A. Paul, and J. D. Thompson, Scaled local gate controller for optically addressed qubits, Optica **11**, 227 (2024).

[37] X. Li, J.-Y. Hou, J.-C. Wang, G.-W. Wang, X.-D. He, F. Zhou, Y.-B. Wang, M. Liu, J. Wang, P. Xu *et al.*, A fiber array architecture for atom quantum computing, Nat. Commun. **16**, 9728 (2025).

[38] D.-Q. Ma, Q.-X. Jie, Y.-D. Hu, W.-Y. Zhu, Y.-C. Zhang, H.-J. Fan, X.-K. Zhong, G.-J. Chen, Y.-L. Zhang, T.-Y. Zhang *et al.*, Volcano architecture for scalable quantum processor units, Sci. China Phys. Mech. Astron. **69**, 220314 (2026).

[39] G. Wang, W. Xu, C. Li, V. Vuletić, and P. Cappellaro, Individual-atom control in an array through phase modulation, Phys. Rev. Appl. **23**, 024072 (2025).

[40] I. Christen, T. Propson, M. Sutula, H. Sattari, G. Choong, C. Panuski, A. Melville, J. Mallek, C. Brabec, S. Hamilton *et al.*, An integrated photonic engine for programmable atomic control, Nat. Commun. **16**, 82 (2025).

[41] L. Li, X. Hu, Z. Jia, W. Huie, W. K. C. Sun, Aakash, Y. Dong, N. Hiri-O-Tuppa, and J. P. Covey, Parallelized telecom quantum networking with an ytterbium-171 atom array, Nat. Phys. **21**, 1826 (2025).

[42] J. P. Covey, H. Weinfurter, and H. Bernien, Quantum networks with neutral atom processing nodes, npj Quantum Inf. **9**, 90 (2023).

[43] L. Hartung, M. Seubert, S. Welte, E. Distante, and G. Rempe, A quantum-network register assembled with optical tweezers in an optical cavity, Science **385**, 179 (2024).

[44] B. Grinkemeyer, E. Guardado-Sanchez, I. Dimitrova, D. Shchepanovich, G. E. Mandopoulou, J. Borregaard, V. Vuletić, and M. D. Lukin, Error-detected quantum operations with neutral atoms mediated by an optical cavity, Science **387**, 1301 (2025).

[45] E. Deist, Y.-H. Lu, J. Ho, M. K. Pasha, J. Zeiher, Z. Yan, and D. M. Stamper-Kurn, Mid-circuit cavity measurement in a neutral atom array, Phys. Rev. Lett. **129**, 203602 (2022).

[46] A. L. Shaw, A. Soper, D. Shadmany, A. Kumar, L. Palm, D.-Y. Koh, V. Kaxiras, L. Taneja, M. Jaffe, D. I. Schuster *et al.*, A cavity-array microscope for parallel single-atom interfacing, Nature (London) **650**, 320 (2026).

[47] Y. Liu, Z. Wang, P. Yang, Q. Wang, Q. Fan, S. Guan, G. Li, P. Zhang, and T. Zhang, Realization of strong coupling between deterministic single-atom arrays and a high-finesse miniature optical cavity, Phys. Rev. Lett. **130**, 173601 (2023).

[48] G. Wang, D. C. Spierings, M. L. Peters, M.-W. Chen, U. Delić, and V. Vuletić, Programmable few-atom Bragg scattering and ground-state cooling in a cavity, arXiv:2508.10748.

[49] Y. Li, Y. Bao, M. Peper, C. Li, and J. D. Thompson, Fast continuous and coherent atom replacement in a neutral atom qubit array, arXiv:2506.15633.

[50] R. Tao, M. Ammenwerth, F. Gyger, I. Bloch, and J. Zeiher, High-fidelity detection of large-scale atom arrays in an optical lattice, Phys. Rev. Lett. **133**, 013401 (2024).

[51] A. Jenkins, J. W. Lis, A. Senoo, W. F. McGrew, and A. M. Kaufman, Ytterbium nuclear-spin qubits in an optical tweezer array, Phys. Rev. X **12**, 021027 (2022).

[52] S. Ma, A. P. Burgers, G. Liu, J. Wilson, B. Zhang, and J. D. Thompson, Universal gate operations on nuclear spin qubits in an optical tweezer array of ^{171}Yb atoms, Phys. Rev. X **12**, 021028 (2022).

[53] A. W. Young, W. J. Eckner, W. R. Milner, D. Kedar, M. A. Norcia, E. Oelker, N. Schine, J. Ye, and A. M. Kaufman, Half-minute-scale atomic coherence and high relative stability in a tweezer clock, Nature (London) **588**, 408 (2020).

[54] I. S. Madjarov, J. P. Covey, A. L. Shaw, J. Choi, A. Kale, A. Cooper, H. Pichler, V. Schkolnik, J. R. Williams, and M. Endres, High-fidelity entanglement and detection of alkaline-earth Rydberg atoms, Nat. Phys. **16**, 857 (2020).

[55] A. L. Shaw, Z. Chen, J. Choi, D. K. Mark, P. Scholl, R. Finkelstein, A. Elben, S. Choi, and M. Endres, Benchmarking highly entangled states on a 60-atom analogue quantum simulator, Nature (London) **628**, 71 (2024).

[56] S. Ma, G. Liu, P. Peng, B. Zhang, S. Jandura, J. Claes, A. P. Burgers, G. Pupillo, S. Puri, and J. D. Thompson, High-fidelity gates and mid-circuit erasure conversion in an atomic qubit, Nature (London) **622**, 279 (2023).

[57] W. J. Eckner, N. Darkwah Oppong, A. Cao, A. W. Young, W. R. Milner, J. M. Robinson, J. Ye, and A. M. Kaufman, Realizing spin squeezing with Rydberg interactions in an optical clock, Nature (London) **621**, 734 (2023).

[58] N. Schine, A. W. Young, W. J. Eckner, M. J. Martin, and A. M. Kaufman, Long-lived bell states in an array of optical clock qubits, Nat. Phys. **18**, 1067 (2022).

[59] J. W. Lis, A. Senoo, W. F. McGrew, F. Rönchen, A. Jenkins, and A. M. Kaufman, Midcircuit operations using the omg architecture in neutral atom arrays, Phys. Rev. X **13**, 041035 (2023).

[60] Y. Wu, S. Kolkowitz, S. Puri, and J. D. Thompson, Erasure conversion for fault-tolerant quantum computing in alkaline earth Rydberg atom arrays, Nat. Commun. **13**, 4657 (2022).

[61] K. Sahay, J. Jin, J. Claes, J. D. Thompson, and S. Puri, High-threshold codes for neutral-atom qubits with biased erasure errors, Phys. Rev. X **13**, 041013 (2023).

[62] P. Scholl, A. L. Shaw, R. B.-S. Tsai, R. Finkelstein, J. Choi, and M. Endres, Erasure conversion in a high-fidelity Rydberg quantum simulator, Nature (London) **622**, 273 (2023).

[63] Y. Fung and M. Andersen, Efficient collisional blockade loading of a single atom into a tight microtrap, New J. Phys. **17**, 073011 (2015).

[64] T. Grünzweig, A. Hilliard, M. McGovern, and M. Andersen, Near-deterministic preparation of a single atom in an optical microtrap, Nat. Phys. **6**, 951 (2010).

[65] M. O. Brown, T. Thiele, C. Kiehl, T.-W. Hsu, and C. A. Regal, Gray-molasses optical-tweezer loading: Controlling collisions for scaling atom-array assembly, Phys. Rev. X **9**, 011057 (2019).

[66] M. M. Aliyu, L. Zhao, X. Q. Quek, K. C. Yellapragada, and H. Loh, D1 magic wavelength tweezers for scaling atom arrays, Phys. Rev. Res. **3**, 043059 (2021).

[67] J. Ang'ong'A, C. Huang, J. P. Covey, and B. Gadway, Gray molasses cooling of ^{39}k atoms in optical tweezers, Phys. Rev. Res. **4**, 013240 (2022).

[68] W. F. Meggers and J. L. Tech, The first spectrum of ytterbium (yb i), J. Res. Natl. Bur. Stand. **83**, 13 (1978).

[69] See Supplemental Material at http://link.aps.org/supplemental/10.1103/bp6k-8zmd for additional information about experimental methods and theoretical analysis, which includes Refs. [70–73].

[70] E. Dennis, A. Kitaev, A. Landahl, and J. Preskill, Topological quantum memory, J. Math. Phys. (N.Y.) **43**, 4452 (2002).

[71] A. G. Fowler, M. Mariantoni, J. M. Martinis, and A. N. Cleland, Surface codes: Towards practical large-scale quantum computation, Phys. Rev. A **86**, 032324 (2012).

[72] Z. Tian, H. Chang, X. Lv, M. Yang, Z. Wang, P. Yang, P. Zhang, G. Li, and T. Zhang, Extending the coherence time limit of a single-alkali-atom qubit by suppressing phonon-jumping-induced decoherence, Optica **11**, 1391 (2024).

[73] K. Barnes, P. Battaglino, B. J. Bloom, K. Cassella, R. Coxe, N. Crisosto, J. P. King, S. S. Kondov, K. Kotru, S. C. Larsen *et al.*, Assembly and coherent control of a register of nuclear spin qubits, Nat. Commun. **13**, 2779 (2022).

[74] F. Nogrette, H. Labuhn, S. Ravets, D. Barredo, L. Béguin, A. Vernier, T. Lahaye, and A. Browaeys, Single-atom trapping in holographic 2D arrays of microtraps with arbitrary geometries, Phys. Rev. X **4**, 021034 (2014).

[75] H. Kim, M. Kim, W. Lee, and J. Ahn, Gerchberg-saxton algorithm for fast and efficient atom rearrangement in optical tweezer traps, Opt. Express **27**, 2184 (2019).

[76] R. W. Gerchberg, A practical algorithm for the determination of phase from image and diffraction plane pictures, Optik (Stuttgart) **35**, 237 (1972).

[77] S. Saskin, J. T. Wilson, B. Grinkemeyer, and J. D. Thompson, Narrow-line cooling and imaging of ytterbium atoms in an optical tweezer array, Phys. Rev. Lett. **122**, 143002 (2019).

[78] A. Muzi Falconi, R. Panza, S. Sbernardori, R. Forti, R. Klemt, O. Abdel Karim, M. Marinelli, and F. Scazza, Microsecond-scale high-survival and number-resolved detection of ytterbium atom arrays, Phys. Rev. Lett. **135**, 203402 (2025).

[79] Z. W. Barber, C. W. Hoyt, C. W. Oates, L. Hollberg, A. V. Taichenachev, and V. I. Yudin, Direct excitation of the forbidden clock transition in neutral ^{174}Yb atoms confined to an optical lattice, Phys. Rev. Lett. **96**, 083002 (2006).

[80] S. Jandura, J. D. Thompson, and G. Pupillo, Optimizing Rydberg gates for logical-qubit performance, PRX Quantum **4**, 020336 (2023).

[81] L. Anderegg, L. W. Cheuk, Y. Bao, S. Burchesky, W. Ketterle, K.-K. Ni, and J. M. Doyle, An optical tweezer array of ultracold molecules, Science **365**, 1156 (2019).

[82] J. T. Zhang, L. R. B. Picard, W. B. Cairncross, K. Wang, Y. Yu, F. Fang, and K.-K. Ni, An optical tweezer array of ground-state polar molecules, Quantum Sci. Technol. **7**, 035006 (2022).

[83] T. Karman and J. M. Hutson, Microwave shielding of ultracold polar molecules, Phys. Rev. Lett. **121**, 163401 (2018).

[84] L. Lassablière and G. Quéméner, Controlling the scattering length of ultracold dipolar molecules, Phys. Rev. Lett. **121**, 163402 (2018).

[85] L. Anderegg, S. Burchesky, Y. Bao, S. S. Yu, T. Karman, E. Chae, K.-K. Ni, W. Ketterle, and J. M. Doyle, Observation of microwave shielding of ultracold molecules, Science **373**, 779 (2021).

[86] A. Schindewolf, R. Bause, X.-Y. Chen, M. Duda, T. Karman, I. Bloch, and X.-Y. Luo, Evaporation of microwave-shielded polar molecules to quantum degeneracy, Nature (London) **607**, 677 (2022).

[87] J. Lin, G. Chen, M. Jin, Z. Shi, F. Deng, W. Zhang, G. Quéméner, T. Shi, S. Yi, and D. Wang, Microwave shielding of bosonic NaRb molecules, Phys. Rev. X **13**, 031032 (2023).

[88] N. Bigagli, C. Warner, W. Yuan, S. Zhang, I. Stevenson, T. Karman, and S. Will, Collisionally stable gas of bosonic dipolar ground-state molecules, Nat. Phys. **19**, 1579 (2023).

[89] F. Deng, X.-Y. Chen, X.-Y. Luo, W. Zhang, S. Yi, and T. Shi, Effective potential and superfluidity of microwave-shielded polar molecules, Phys. Rev. Lett. **130**, 183001 (2023).

[90] J. Zhu, C. Chen, L. Zhou, X. Xie, C. Jiang, Z. Ding, F. Wu, F. Yang, G. Wang, Q. Gong *et al.*, 10.5281/zenodo.21289872 (2026).